Recognizing different tissues in human fetal femur cartilage by label-free Raman microspectroscopy

Aliz Kunstar
Jeroen Leijten
Stefan van Leuveren
Janneke Hilderink
Cees Otto
Clemens A. van Blitterswijk
Marcel Karperien
Aart A. van Apeldoorn

SPIE

Recognizing different tissues in human fetal femur cartilage by label-free Raman microspectroscopy

Aliz Kunstar,[a] **Jeroen Leijten,**[a,b] **Stefan van Leuveren,**[a] **Janneke Hilderink,**[a,b] **Cees Otto,**[c] **Clemens A. van Blitterswijk,**[a] **Marcel Karperien,**[a,b] **and Aart A. van Apeldoorn**[a,b]

[a]University of Twente, MIRA—Institute for Biomedical Technology and Technical Medicine, Department of Tissue Regeneration, Drienerlolaan 5, 7522 NB Enschede, The Netherlands
[b]University of Twente, MIRA—Institute for Biomedical Technology and Technical Medicine, Department of Developmental Bioengineering, Drienerlolaan 5, 7522 NB Enschede, The Netherlands
[c]University of Twente, MIRA—Institute for Biomedical Technology and Technical Medicine, Department of Medical Cell Biophysics, Drienerlolaan 5, 7522 NB Enschede, The Netherlands

Abstract. Traditionally, the composition of bone and cartilage is determined by standard histological methods. We used Raman microscopy, which provides a molecular "fingerprint" of the investigated sample, to detect differences between the zones in human fetal femur cartilage without the need for additional staining or labeling. Raman area scans were made from the (pre)articular cartilage, resting, proliferative, and hypertrophic zones of growth plate and endochondral bone within human fetal femora. Multivariate data analysis was performed on Raman spectral datasets to construct cluster images with corresponding cluster averages. Cluster analysis resulted in detection of individual chondrocyte spectra that could be separated from cartilage extracellular matrix (ECM) spectra and was verified by comparing cluster images with intensity-based Raman images for the deoxyribonucleic acid/ribonucleic acid (DNA/RNA) band. Specific dendrograms were created using Ward's clustering method, and principal component analysis (PCA) was performed with the separated and averaged Raman spectra of cells and ECM of all measured zones. Overall (dis)similarities between measured zones were effectively visualized on the dendrograms and main spectral differences were revealed by PCA allowing for label-free detection of individual cartilaginous zones and for label-free evaluation of proper cartilaginous matrix formation for future tissue engineering and clinical purposes. © *2012 Society of Photo-Optical Instrumentation Engineers (SPIE).* [DOI: 10.1117/1.JBO.17.11.116012]

1 Introduction

Fetal long bones consist of (pre)articular cartilage, growth plate cartilage, and bone tissue. Together, they regulate longitudinal bone growth and long bone development. (Pre)articular cartilage, also referred to as the proximal resting zone, will eventually become articular cartilage and is located several cell layers below the joint surface. Fetal long bones differ from postnatal long bones in that they do not possess a secondary center of ossification. Moreover, their growth plates are much thicker and the chondrocytes are more compactly located.[1] In general, the growth plate can be subdivided into four distinct zones: the resting zone, the proliferative zone, the prehypertrophic zone, and the hypertrophic zone. Resting zone chondrocytes are small, uniform and compactly positioned and are characterized by low rates of proliferation and synthesis of proteoglycans and collagen type IIB.[2,3] In the proliferative zone, the chondrocytes have an increased proliferation rate that results in the formation of longitudinal columns. In addition, this zone has increased collagen type II and XI synthesis.[1] Following this zone is the prehypertrophic zone, where chondrocytes lose their ability to proliferate and gradually increase in size due to swelling. In the hypertrophic zone, a cascade of events is triggered

including ECM mineralization, angiogenesis, and apoptosis of chondrocytes.[1]

Current knowledge regarding the composition of the different zones is mainly based on histology,[4] immunohistochemistry,[5] *in situ* hybridization,[6,7] and electron microscopy.[8] However, these methods do not yield direct information on the molecular composition of the investigated samples. Therefore, elucidating the molecular compositions of the different cartilage zones can result in a deeper understanding of the changes underlying terminal differentiation of chondrocytes, which drives the development of long bones. Raman spectroscopy is an analytical technique able to measure the molecular composition by providing a spectrum that contains information regarding all the chemical bonds present within the sample. As opposed to histology and immunohistochemistry, which only provides information regarding the presence of specific compounds, Raman spectroscopy creates a "fingerprint" representing the entire molecular composition of the sample. Raman spectroscopy is based on the inelastic light scattering effect, in which one in a million photons is scattered with a different wavelength than the incident photons following interaction with the sample.[9–12] The wavelength shift is specific for the chemical bond where the photon is emitted. By detecting all the photons with a shifted wavelength, a Raman spectrum can be constructed. It has been demonstrated that a careful selection of

Address all correspondence to: Aart A. van Apeldoorn, University of Twente, MIRA—Institute for Biomedical Technology and Technical Medicine, Department of Tissue Regeneration, Drienerlolaan 5, 7522 NB Enschede, The Netherlands. Tel.: +31-53-489-2153/3400; Fax: +31-53-489-2150; E-mail: a.a.vanapeldoorn@utwente.nl

suitable laser wavelength and laser intensity eliminates the possibility of cell damage.[13,14] Since the first application of Raman spectroscopy on cells, this technique has been widely used for biological applications.[15]

In this study, different zones of human fetal femoral tissue were studied with Raman microspectroscopy. In order to be able to compare Raman results to histological data, all experiments were performed on cryosections. The aim of this study was to determine whether confocal Raman microspectroscopy is able to effectively discriminate between different cartilaginous zones of a developing diarthrodial joint and to identify the molecular differences between the (pre)articular cartilage and the different zones of the growth plate cartilage. Together, this knowledge contributes to our understanding on how to generate a specific type of cartilage for future tissue engineering and clinical purposes.

2 Experimental Section

2.1 Sample Preparation

Bovine articular cartilage pieces were obtained from the femoral-patellar groove of a 10-week-old calf, fixed in 10% formalin for 10 min and washed in phosphate-buffered saline (PBS, Gibco). After consent and medical ethical committee permission for use of human fetal material had been obtained, fetal femurs were isolated from three human fetuses undergoing elective termination of pregnancy with 20 weeks of gestation. Femurs were snap-frozen in liquid nitrogen and stored at −80°C until processing. The samples were embedded in cryomatrix (Shandon Cryomatrix, Thermo Scientific), frozen to −49°C, sectioned at 20 μm thickness at −19°C using a cryomicrotome (Shandon Cryotome 77210160, Thermo Scientific), and placed on UV grade calcium fluoride (CaF_2) slides (Crystran Ltd.). Before Raman measurements, the cryosections of the human fetal femur were fixed in 10% formalin for 10 min and extensively washed with PBS and the cryosections of bovine articular cartilage were extensively washed with PBS.

2.2 Histology

The embedded samples of the fetal femora were sectioned at 8 μm thickness using the cryomicrotome and stained with Safranin-O (Sigma) for visualization of sulfated glycosaminoglycans (sGAGs), hematoxylin and eosin (H&E, Sigma) for visualization of the nuclei and cytoplasm, and Alizarin Red S (Sigma) for visualization of calcification.

2.3 Confocal Raman Microspectroscopy

Raman measurements were performed using a home-built confocal Raman spectrometer as previously described.[16–18] Briefly, a Krypton ion laser (Coherent, Innova 90K) with an emission wavelength of 647.1 nm was used as the excitation source. An air objective (Olympus UIS2, UPlanFLN, Olympus, 40x, 0.75 NA) was used to illuminate the sample as well as to collect the Raman-scattered photons in the epi-detection mode. The scattered light was filtered by a razor-edge filter (Semrock, Rochester) to suppress reflected laser light and Rayleigh-scattered light, and focused onto a pinhole of 15 μm diameter at the entrance of an imaging spectrograph/monochromator (HR460; Jobin-Yvon), which contains a blazed holographic grating with 600 grooves/mm. The spectrograph disperses the Raman-scattered photons on an air-cooled electron-multiplying

charge-coupled device (EMCCD, Newton DU-970N, Andor Technology). The system provided a spectral resolution of 1.85 to 2.85 cm^{-1}/pixel over the wavenumber range from −20 to 3670 cm^{-1}. The samples were scanned by using a scanning mirror system (SM, MG325D and G120D, General Scanning). Raman spectra were acquired in the so-called "spectral scanning mode" for: 1. washed cryosection with bovine articular cartilage, 2. unwashed cryosection without cartilage, and 3. washed cryosection without cartilage. In this measurement mode, a single full spectrum is obtained by raster scanning the laser beam with a laser power of 35 mW over an area of 30 × 30 μm in 30 s. Raman images were acquired from cryosections of human fetal femurs by recording a full spectrum from each position of the laser beam guided by the displacement of the scanning mirror in the area of interest on the samples. These measurements were performed in an area of 30 × 30 μm with an accumulation time of 1 s/step and an excitation power of 35 mW. The laser spot size used in this study was 310 nm. The 30 × 30 μm area scans were made with 30 μm distance adjacent from each other, by using a Kleindiek substage LT6820 controlled by a Kleindiek NanoControl (Kleindiek Nanotechnik), in such a way that the total area of 120 × 120 μm could be constructed from these initial scans. After data correction, the scans of 30 × 30 μm of fetal femur samples resulted in 256 spectra each, which were subsequently combined into areas of 120 × 120 μm consisting of 4096 spectra from each zone in the human fetal femur. Toluene, a Raman calibration standard with accurately known peak frequencies (521, 785, 1004, 1624, 2921, and 3054 cm^{-1}) was used for wavenumber calibration of the spectra.

2.4 Raman Data Analysis

Preprocessing of the data was performed as described in the literature (see Refs. 17, 19, and 20). Briefly, the spectra were preprocessed by: 1. removing cosmic ray events, 2. subtracting the camera-offset noise (dark current), and 3. calibrating the wavenumber axis. Cosmic rays, identified as nonspecific high intensity spikes in the acquired signal with an average width of 1 to 4 pixels and intensity much higher than the detected Raman signal, were removed from the signal using an estimation of the first derivative of the signal and setting a threshold accordingly.[21] The well-known band-positions were used to relate wavenumbers to pixels. The frequency-dependent optical detection efficiency of the setup was corrected using a tungsten halogen light source (Avalight-HAL; Avantes BV) with a known emission spectrum. Also, the detector-induced etaloning effect was compensated by this procedure.

Singular value decomposition (SVD) was applied to the hyperspectral data cubes (consisting of 4096 spectra) to reduce the uncorrelated noise resulting in the raw 3D data matrix after converting them to 2D matrix.[22] The SVD-treated data were analyzed by multivariate data analysis procedures. In multivariate analysis, both principal component analysis (PCA) and hierarchical cluster analysis (HCA) were performed on the datasets resulting in cluster images and corresponding cluster averages. HCA made use of the scores obtained from the PCA to visualize the regions containing high spectral similarities. HCA is an unsupervised cluster analysis method, which resulted in separation of cell spectra from ECM spectra. Cell clusters and ECM clusters were arranged in separate databases and dendograms were made using Ward's clustering method (HCA) based on Euclidean inter-point distances.[23] Squared Euclidean distances as distance measure and Ward's algorithm to separate Raman

spectra into clusters were used. The influence of small variations in the baseline was minimized by preprocessing data with a first derivative Savitsky-Golay algorithm, which was implemented as a seven point smoothing and a quadratic polynomial fit.[24,25] The data was further autoscaled to the mean of the spectra along the frequency axis.[24,25] Additionally, PCA analysis was performed on the separated cell and ECM cluster averages. PCA is a mathematical reduction of the dimensionality of the measurement matrix into fewer variables (principal components) and describes the most significant variance between the data.[25,26]

All data manipulations were performed using routines written in MATLAB 7.4 (MathWorks). Ward's clustering and PCA analysis on the separated cell and ECM cluster average spectra were performed using PLS toolbox (Eigenvectors Research Inc.) in MATLAB 7.8.

3 Results and Discussion

The aim of this study was to determine whether confocal label-free Raman microspectroscopy is able to effectively discriminate between various tissues, particularly between (pre)articular cartilage and growth plate cartilage of human fetal femur. Detailed understanding of the molecular composition might prove essential in the quest to generate a specific type of cartilage and to identify molecular markers to distinguish between these two types of cartilage for future tissue engineering and clinical purposes.

3.1 Histology

In order to demonstrate the healthy and unaffected nature of the fetal femur, we subjected 8 μm thick cryosections to histological

analysis using Alizarin Red S, Safranin-O, and H&E staining. The results of the histological staining were demonstrated in Fig. 1. Alizarin Red S staining confirmed that (pre)articular cartilage, resting, and proliferative zone cartilage did not contain any detectable levels of calcification. As expected, the terminal areas of the hypertrophic zone showed mild levels of calcification. Moreover, the entire matrix of the endochondral bone was intensely stained for calcification. Safranin-O staining visualized sGAGs, one of the major components of the ECM. In the (pre)articular cartilage and resting zone of growth plate, abundant sGAG deposition was observed. Light microscopy confirmed that in the proliferative zone the ECM to cell ratio decreased. In the hypertrophic zone, the ratio of ECM to cell further decreased. In the endochondral bone, no detectable amounts of sGAGs were present. With the H&E staining, it was demonstrated that the cells in the (pre)articular cartilage and resting zone were very small and compactly located, while in the proliferative zone they were increased in size and the column-like structure of the cells were clearly visible. In the hypertrophic zone, the cells had greatly increased in size and only a small amount of ECM formation was observed. The endochondral bone appeared quite similar to the hypertrophic zone. The combined histological analysis demonstrated the healthy nature of the specimen and allowed for distinct localization of the various zones.

3.2 Confocal Raman Microspectroscopy

It has previously been reported that the use of paraffin prohibits the acquisition of useful Raman measurements.[27] In contrast, it has been shown that the use of cryomatrix, after washing the tissue cryosections with PBS, does not interfere with Raman
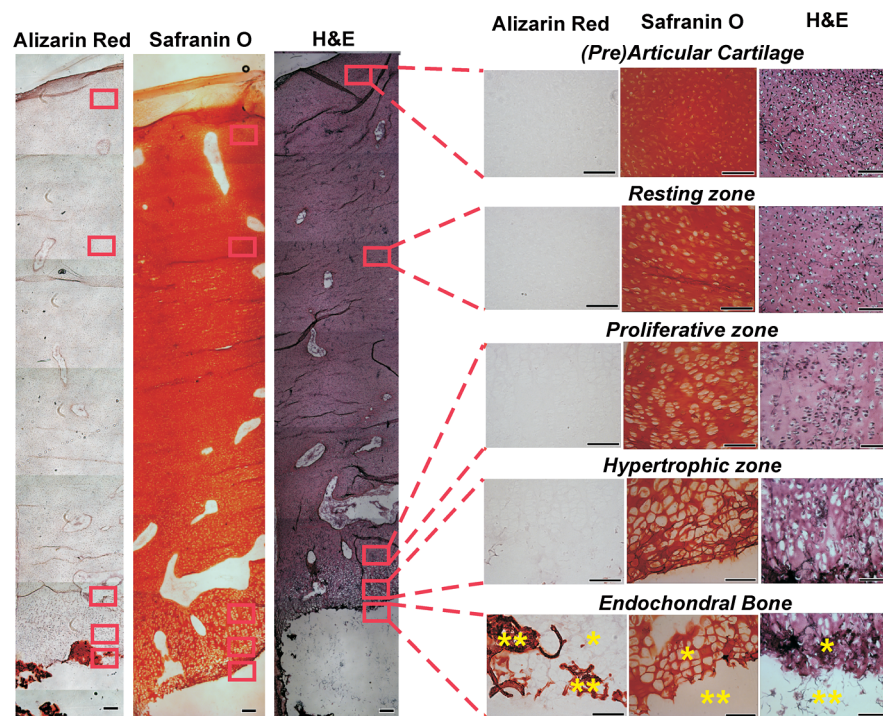

Fig. 1 Histological analysis of human fetal femurs: Alizarin Red S staining visualized calcification, Safranin O staining visualized sGAGs, and hematoxylin and eosin (H&E) staining visualized nuclei and cytoplasm. In the detailed images of the endochondral bone, the distal part of terminal hypertrophic zone can also be observed (the terminal hypertrophic zone part is labeled with a star and the endochondral bone part with two stars). The boundary between the terminal hypertrophic and endochondral bone part is irregular. The overview scans were made with a 4× objective and scale bars equal 200 μm. The detailed scans were made with a 20× objective and scale bars equal 100 μm.
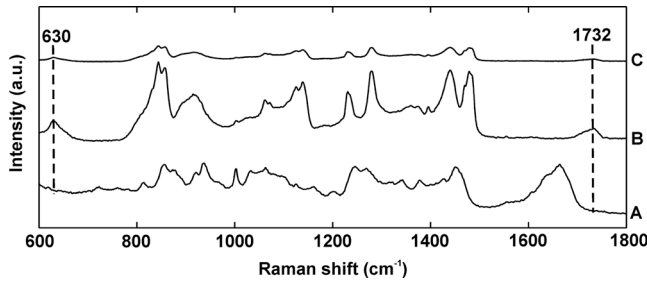
Fig. 2 Raman spectra of cryosections with and without cartilage sample. (a) Washed cryosection with bovine articular cartilage, (b) unwashed cryosection without cartilage, and (c) washed cryosection without cartilage in the range of 500 to 1800 cm^{-1} acquired in the so-called "spectral scanning mode." The spectra were identically scaled and vertically displaced for clarity.

measurements.[28] Therefore, in this study, cryomatrix was used to embed tissue samples and cryosections were prepared for Raman measurements. In addition, CaF_2 slides were used as a substrate of the tissue sections for all the Raman measurement to avoid background signal. Compared with the Raman spectrum of washed cartilage section [Fig. 2(a)], both the spectra of the unwashed [Fig. 2(b)] and washed [Fig. 2(c)] cryomatrix (without cartilage) showed Raman bands in the same regions, except the Raman bands at 630 and 1732 cm^{-1}. These peaks could be assigned to glycerol[29] and poly(vinyl alcohol) (PVA),[30] respectively, which are the major compounds of the cryomatrix. The lack of these two peaks in the Raman spectrum of washed cartilage section indicated cryomatrix did not interfere with the cartilage measurements.

Raman spectroscopic studies of native cartilage have mainly focused on direct analysis of ECM components. Raman analysis has been performed for the analysis of collagen in the sclera, articular cartilage, and subchondral bone of wild-type and transgenic mice harboring structural truncations in the introduced collagen type II transgene.[31] Moreover, Raman microspectroscopic mapping studies have already been carried out on human bronchial tissue.[32] FTIR spectroscopy is usually a more common tool to study articular cartilage. For example, it has been demonstrated in literature that FTIR imaging can assess changes in composition and distribution of ECM components in human osteoarthritic cartilage.[33]
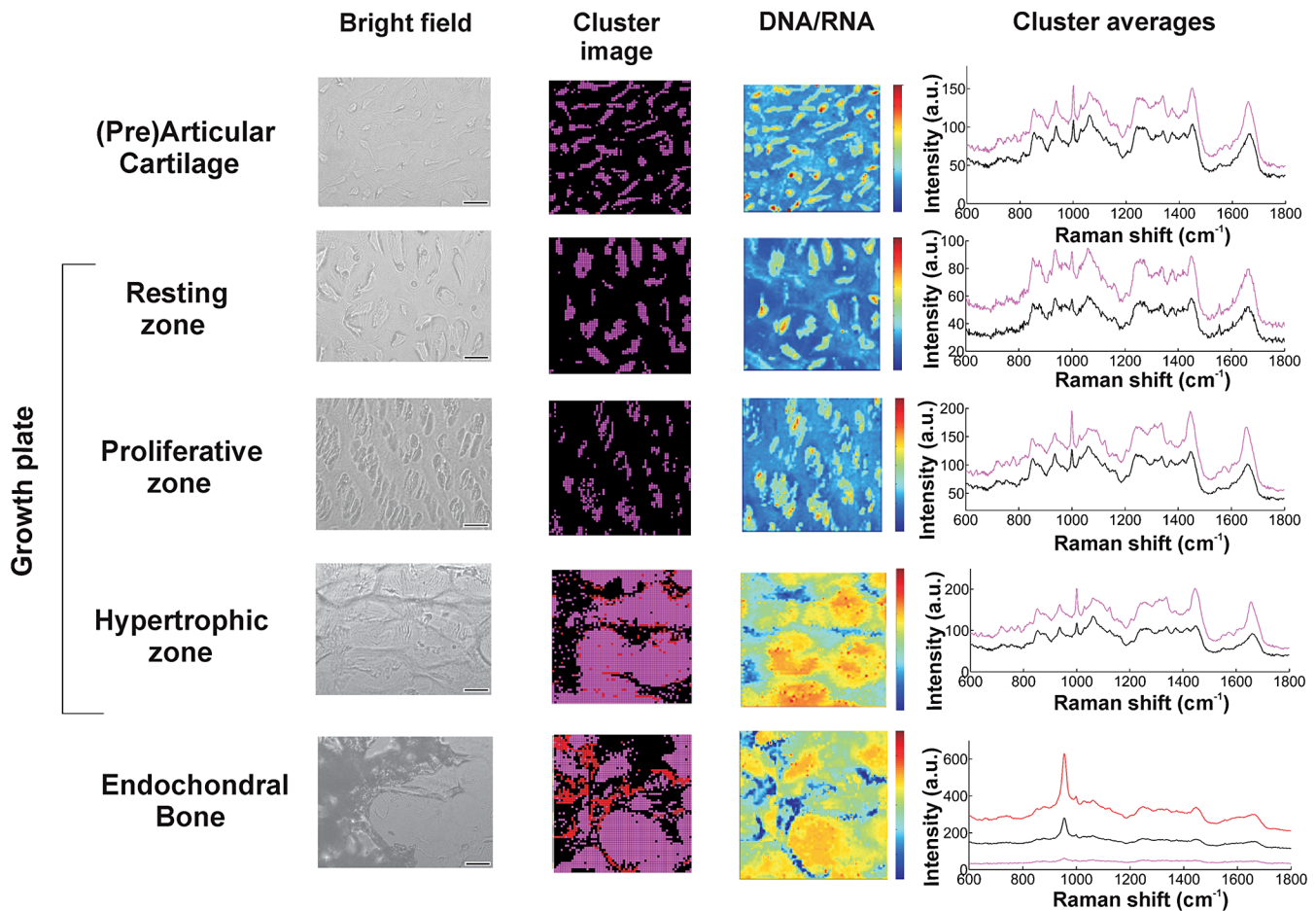

Fig. 3 Bright field images, cluster images with corresponding Raman cluster averages from cells and ECM, and Raman images from the (pre)articular cartilage, the resting, proliferative, and hypertrophic zone of the growth plate and the endochondral bone from the human fetal femur. Raman images were focused on the intensity of the DNA/RNA band at 1576 cm^{-1}. The highest (red) intensity of this band can be observed within the cells in all the zones. Each cluster average spectrum is corresponding to the cluster with the same color in the cluster images (purple spectrum of the cluster averages is corresponding to the purple clusters in the cluster image). The purple clusters are corresponding to cell clusters and the black clusters to ECM clusters in all the zones of the fetal femur. In the endochondral bone, two clusters, the black and the red, are representing the ECM clusters, which can be explained by the heterogeneous character of the ECM in this region. In the hypertrophic zone, the red clusters were fluorescent background noise, therefore they were removed from the cluster averages and were not used for further data analysis. The truncated and separated cluster averages are also demonstrated in Fig. 4 (cells) and Fig. 5 (ECM) in more detail for further observation. Scale bars on the bright field images equal 20 μm.

In this study, Raman measurements on human fetal femur samples were performed on the areas highlighted in Fig. 1 and on sections consecutive to the sections used for histological analysis. Bright field images (in the bright field mode of the Raman microscope) were obtained from (pre)articular cartilage, resting, proliferative, and hypertrophic zones of the growth plate and the endochondral bone from human fetal femora corresponded with the respective zones demonstrated with conventional histological analysis (Figs. 1 and 3). Raman scans representative of $120 \times 120 \ \mu m$ were made in the same zones as the observed ones in the depicted bright field images. Cluster images with the corresponding cluster averages were obtained from each area (Fig. 3). Hierarchical clustering separated Raman spectra of cells from Raman spectra of ECM. This was verified by comparing hierarchical cluster images with intensity-based Raman images for DNA/RNA bands at 1576 cm^{-1} (Fig. 3). The intensity-based Raman images showed a high DNA/RNA concentration at the same locations as the purple clusters in the cluster images and could be shown as separate clusters in each hierarchical cluster image, which confirms that cells and ECM can be effectively separated based on their respective Raman spectra.

For further data analysis, cluster averages corresponding to cells or ECM were combined in separate databases, thus creating one database specific for all cell cluster averages and one database specific for all ECM cluster averages of each zone. All cell cluster averages showed well-described bands corresponding to collagen,[34] phenylalanine,[35] chondroitin sulfate and proteoglycans (including aggrecan),[36–38] lipids/proteins (CH_2 bending mode[39] and amide I[40,41]), and DNA/RNA[42,43] (Table 1).

Comparing the cell cluster averages with the ECM cluster averages, the most notable difference was the Raman peak of the DNA/RNA at 1576 cm^{-1}, which was clearly visible in all the cell-spectra [Fig. 4(a)], while it was absent in all the ECM spectra (Fig. 5). This supported our assumption that the cells and ECM could be separated based on their Raman spectra for further analysis. Raman images from (pre)articular cartilage focused on the intensity of the DNA/RNA peak at 1576 cm^{-1} was also demonstrated in Fig. 4(b). As expected, the highest intensity (red) of the DNA/RNA peak was observed inside the cells. Except for the DNA/RNA band and differences in band intensities, for example the more intense proteoglycan peaks in ECM spectra, also represented by the Raman images in Fig. 6, cell and ECM spectra had identical peaks. All the cluster averages from the cells showed relatively identical Raman
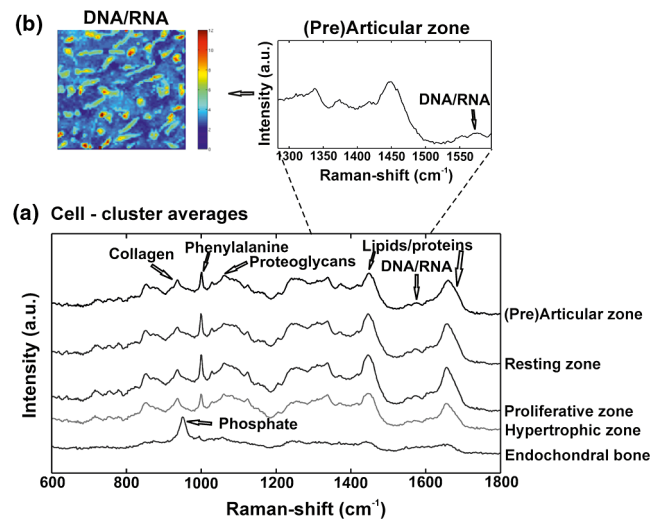

Fig. 4 Raman cluster averages of cells. (a) Average Raman spectra of cells from the (pre)articular cartilage, the resting, proliferative, and hypertrophic zone, and the endochondral bone in the region from 600 to 1800 cm^{-1}. The spectra were vertically displaced for clarity. Truncated Raman spectra from the (pre)articular zone represented in the region from 1300 to 1600 cm^{-1}. (b) Raman image from (pre)articular cartilage focused on the intensity of the DNA/RNA peak at 1576 cm^{-1}.

peaks, except for the peak in the spectrum of the endochondral bone cell presented at 954 cm^{-1} [Fig. 4(a)]. As expected, this peak was undetectable in cell spectra from other zones, but appeared as a very intense peak in the spectra of endochondral bone ECM and as a less intense band in the hypertrophic zone ECM spectra (Fig. 5). This peak is representative for $PO_4^{3-} \ v_1$

Table 1 Assignments and wavelengths for Raman peaks.

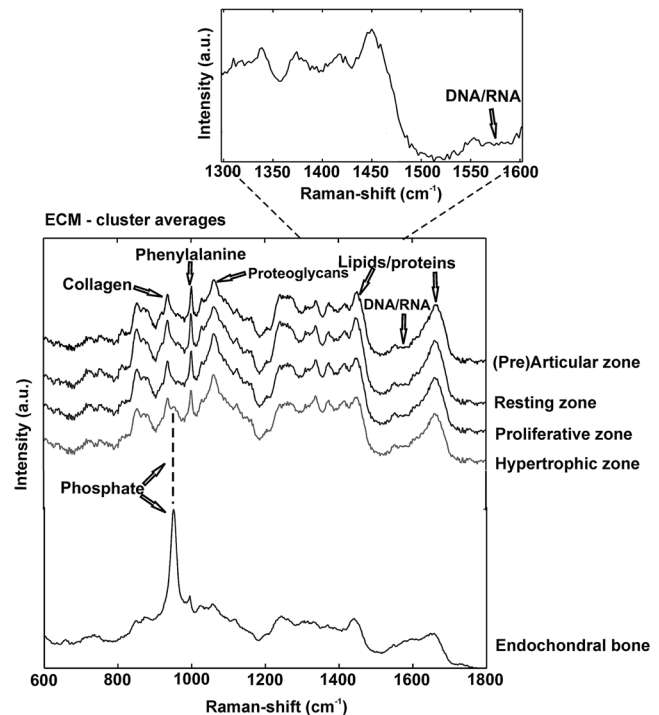| Assignment	Wavelength in cm^{-1} (References)
Collagen (proline/hydroxyproline/ C-C skeletal of collagen backbone	937 (34)
Phosphate (PO_4^{3-})	954 (44)
Phenylalanine (C-C aromatic ring)	1001 (35)
Chondroitin sulfate and proteoglycans	1062 (36, 37, 38)
Lipids/proteins (CH_2 and amide I)	1448 (39) and 1656 (40–41)
DNA/RNA (Guanine-N_3)	1576 (42–43)

Fig. 5 Raman cluster averages of ECM. Average Raman spectra of ECM from the (pre)articular cartilage, the resting, proliferative, and hypertrophic zone, and the endochondral bone in the region from 600 to 1800 cm^{-1}. The spectra were vertically displaced for clarity. Truncated Raman spectrum from the (pre)articular zone represented in the region from 1300 to 1600 cm^{-1}.
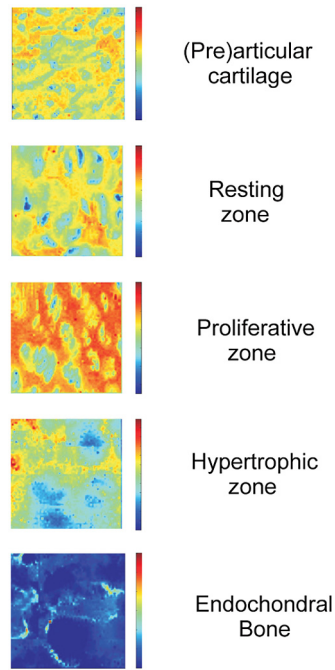
Fig. 6 Intensity based Raman images, focused on the Raman band corresponding to proteoglycans at 1062 cm^{-1}, from the (pre)articular cartilage, the resting, proliferative, and hypertrophic zone of the growth plate, and the endochondral bone from the human fetal femur. The highest intensity was observed in the ECM in all the zones.

symmetric vibration, which is a marker for calcification of the ECM.[44] As expected, these results indicate milder levels of mineralization in the hypertrophic zone ECM than in the endochondral bone ECM, which was also shown by Alizarin Red S staining in Fig. 1 and can be correlated with well-known biochemical differences between these zones of the fetal femur.

In addition, Ward's clustering method (HCA) on cell and ECM cluster averages from all the three donors was used to create dendrograms (Fig. 7) of which representative examples of each individual donor can be seen in Figs. 8, 9, and 10. Raman mapping in combination with multivariate data analysis was previously shown to be successful for the analysis of porcine articular cartilage and used to distinguish between three major zones (superficial, middle, and deep zone) based on major ECM components like collagen and chondroitin-sulfate and noncollagenous proteins.[37]

The dendrogram in Fig. 7(a) shows the clustering of Raman average spectra of the cells from the different zones of the human fetal femora. Before HCA, cell spectra from all three donors were averaged, and the smaller the variance-weighted distance between the cluster centers was, the more they resembled each other. Starting from the right side of the dendrogram, the first two clusters resulted in grouping of spectra corresponding to: 1. (pre)articular cartilage and resting zone cells, and 2. hypertrophic zone, proliferative zone, and endochondral bone cells. The first node separated the spectra corresponding to endochondral bone cells from the cluster of the hypertrophic zone and proliferative zone cells. Since cells in the hypertrophic zone and in the proliferative zone proliferate rapidly, one might expect these cells to have a different chemical composition than the (pre)articular cartilage and resting zone cells, which were in a relatively quiescent state.[1] The differences between chondrocytes and bone cells would include the expression of different genes and therefore different RNAs and intracellular proteins. Some of the DNA and RNA Raman band positions are unique for certain nucleotides,[41,45] and could therefore help to discriminate between different cell types. The second node separated the spectra corresponding to the (pre)articular cartilage from the resting zone cells. The third cluster involved all the spectra from the hypertrophic zone and proliferative zone cells. The dendrogram in Fig. 7(b) shows the clustering of the Raman average spectra of the ECM from the measured zones of the fetal femur. Before HCA, the ECM spectra from all three donors were averaged. As expected, endochondral bone ECM with calcium deposition resembled the least with ECM of all other cartilaginous zones. Moreover, proliferative zone ECM better resembled the hypertrophic zone ECM than the (pre)articular cartilage and resting zone ECM.

After performing HCA, a more elaborate investigation explored the origin of the established dissimilarities in order to find Raman markers identifying molecular differences between the (pre)articular cartilage and growth plate cartilage. In order to find these markers, PCA was performed on the separated cell and ECM cluster average spectra. This method has already been applied for monitoring spectral differences in mRNA translation of embryonic stem cells during differentiation.[25] This type of

Dendrograms of Data with Preprocessing: 1st Derivative (order:4, window: 7pt) + Autoscale
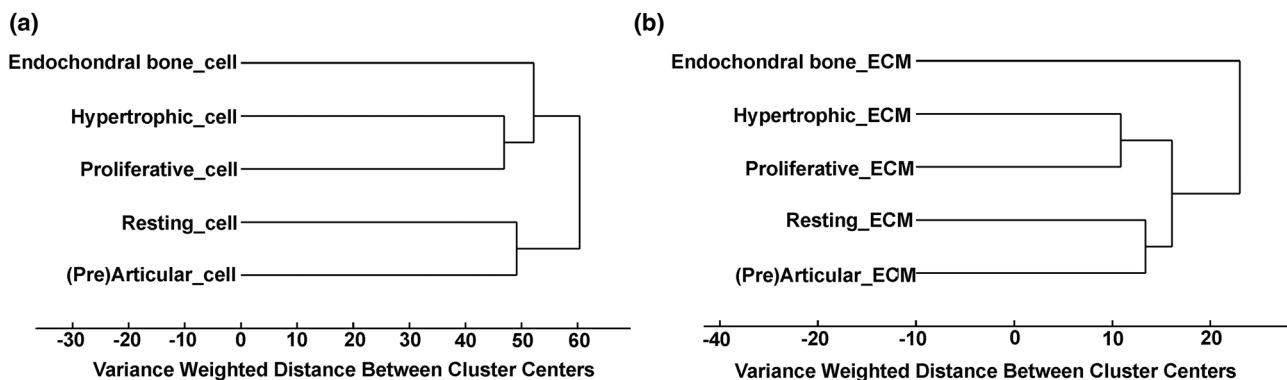

Fig. 7 HCA analysis by Ward's clustering method of Raman average spectra from (a) cells and (b) ECM acquired from the measured zones of the human fetal femur. Each cluster shows grouping of spectral information based on the different zones of the human fetal femur: (pre)articular cartilage, the resting, proliferative, and hypertrophic zone, and the endochondral bone.
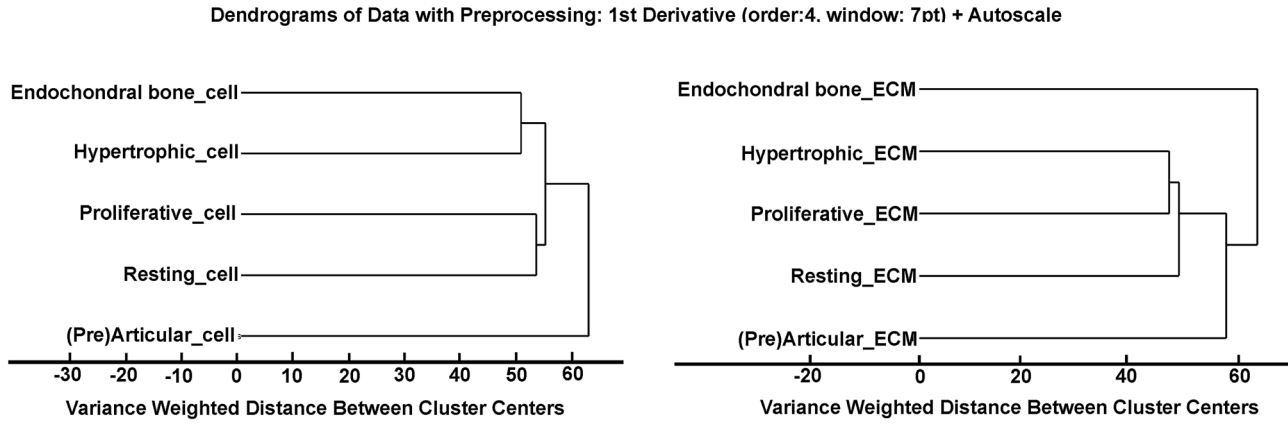
Dendrograms of Data with Preprocessing: 1st Derivative (order:4, window: 7pt) + Autoscale

Fig. 8 HCA analysis by Ward's clustering method of Raman average spectra from cells and ECM acquired from the measured zones of the human fetal femur of Donor 1.

Dendrograms of Data with Preprocessing: 1st Derivative (order:4, window: 7pt) + Autoscale

Fig. 9 HCA analysis by Ward's clustering method of Raman average spectra from cells and ECM acquired from the measured zones of the human fetal femur of Donor 2.
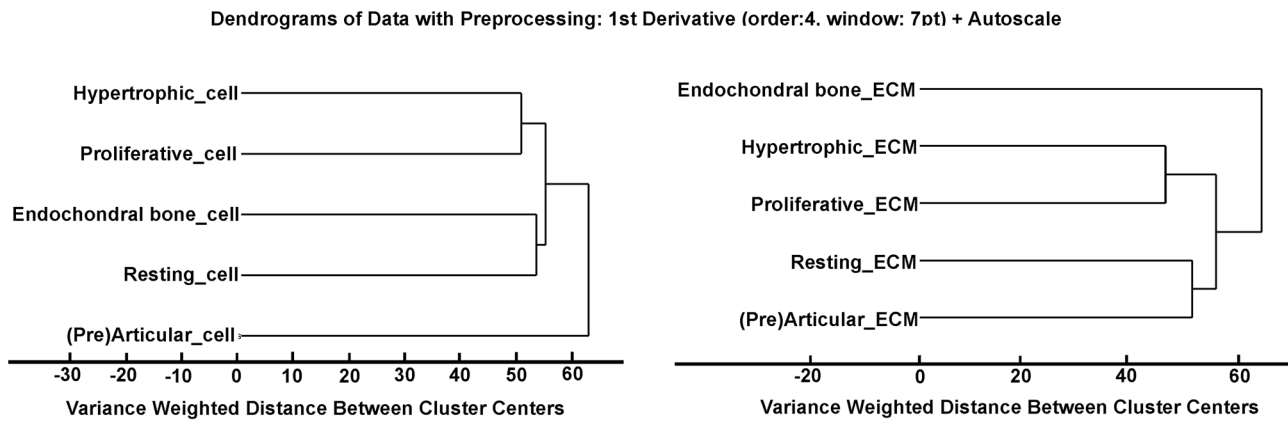
Dendrograms of Data with Preprocessing: 1st Derivative (order:4, window: 7pt) + Autoscale

Fig. 10 HCA analysis by Ward's clustering method of Raman average spectra from cells and ECM acquired from the measured zones of the human fetal femur of Donor 3.
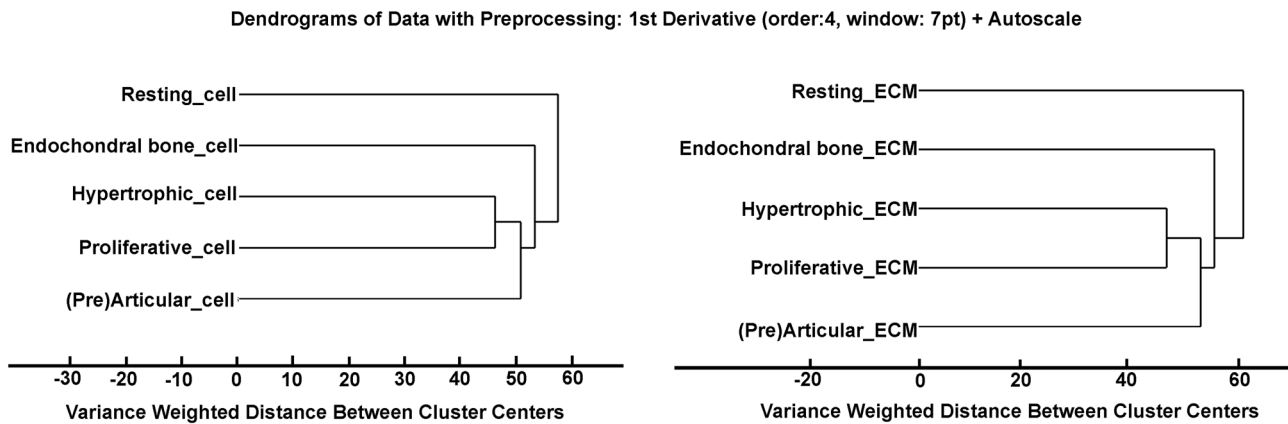
analysis allows the interpretation of similarities and differences between the clusters of the samples by analyzing the PCA scores and loadings.[25] In Raman spectroscopy, the PCA loadings are combinations between Raman spectra of components of the sample that describe the biggest difference between spectra.[25]

By analyzing the cell-cluster averages by PCA [Fig. 11(a) and 11(b)] and utilizing mean-centering on all the spectra as pre-processing, the first principal component gave 72.44% of the

variance and described the difference between the (pre)articular cartilage cells and cells from the zones of the growth plate. (Pre) articular cartilage cells were characterized by high positive values of PC1 scores (endochondral bone cells had low positive values), while cells from the resting, proliferative, and hypertrophic zones had negative scores [Fig. 11(a)]. The PC1 loading spectrum resembled the spectrum of intracellular proteins and lipids with characteristic peaks for collagen at 937 cm^{-1},
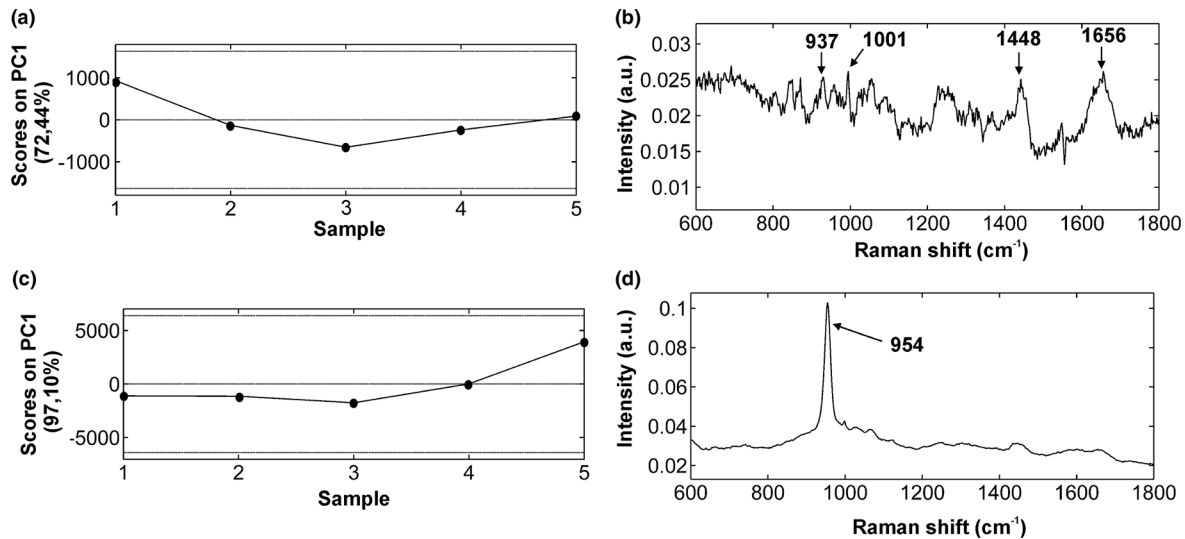
Fig. 11 PCA analysis. (a) PC1 scores of cells from different zones of the fetal femur (1: (pre)articular cartilage cells, 2: resting zone cells, 3: proliferative zone cells, 4: hypertrophic zone cells, and 5: endochondral bone cells). (b) PC1 loading from PCA analysis of cell cluster averages. The PC1 loading spectrum resembled the spectra of intracellular proteins. (c) PC1 scores of ECM from different zones of the fetal femur [1: (pre)articular cartilage ECM, 2: resting zone ECM, 3: proliferative zone ECM, 4: hypertrophic zone ECM, and 5: endochondral bone ECM]. (d) PC1 loading from PCA analysis of ECM cluster averages. The PC1 loading spectrum showed the strongest peak at 954 cm^{-1} corresponding to phosphate.

phenylalanine at 1001 cm^{-1}, CH$_2$ bending mode (lipids/proteins) at 1448 cm^{-1}, and amide I (lipids/proteins) at 1656 cm^{-1} [Fig. 11(b)]. The spectrum of the PC1 loading showed that main differences between the (pre)articular cartilage cells and cells from the zones of the growth plate originate from differences in intracellular protein levels. By analyzing the ECM-cluster averages by PCA [Fig. 11(c) and 11(d)], utilizing mean-centering on all the spectra as preprocessing, the first principal component gave 97.10% of the variance and described the difference between endochondral bone ECM and ECM from the rest of the zones of fetal femur. (Pre)articular cartilage, resting zone, and proliferative zone ECM was characterized by negative values of PC1 scores, while endochondral bone ECM had high positive scores [Fig. 11(c)]. The PC1 loading spectrum showed the strongest peak at 954 cm^{-1}, corresponding to phosphate in the ECM [Fig. 11(d)]. This result showed that the phosphate content of the endochondral bone ECM was the major contributor for biochemical differences between endochondral bone and the rest of the zones. The hypertrophic zone ECM was found to have low positive scores, indicating a mild level of phosphate production (onset of mineralization) in the ECM of this zone. These results are in contrast to what was recently described in a study on adult articular cartilage, in which the authors measured the collagen proline bands at 817 and 921 cm^{-1} to describe the distinction between the superficial and deep zones.[38] However, in our study of fetal articular cartilage, we also included the endochondral zone, allowing for an elaboration of the differences within the hypertrophic zone.

4 Conclusion

Unlike histology and immunohistochemistry, which only give information on the presence of specific compounds, Raman microspectroscopy provides a "fingerprint" representing the entire molecular composition of the zones in human fetal femur. We were able to distinguish bands specific for collagen, phosphate, phenylalanine, DNA/RNA, and amide I. Although unique single difference Raman markers could not be detected in the cartilaginous zones of the femora, the overall (dis)

similarities between measured zones were effectively visualized using dendrograms created by Ward's clustering method. Hierarchical clustering of spectra from different zones in the dendrograms could be related to well-known biochemical differences between cells and ECM from different zones. Furthermore, the main spectral differences could be also determined by analyzing the PCA scores and loadings obtained from the PCA analysis of separate cell and ECM cluster average spectra of the different zones. Therefore, these results show the possibility of label-free Raman microspectroscopy to distinguish between the various cartilage tissues in the human fetal femur cartilage. In addition, it shows its potential to study cartilaginous matrix formation for future tissue engineering and clinical purposes. In cartilage tissue engineering, the occurrence of hypertrophy in tissue-engineered constructs during *in vitro* generation of hyaline cartilage is a well-described problem. Identifying label-free Raman markers for hypertrophy and distinguishing between (pre)articular and growth plate (more specifically cartilage of the hypertrophic zone) cartilage by cluster analysis of Raman spectra from these zones could provide an excellent method for monitoring the quality of cartilage transplants.

References

1. R. T. Ballock and R. J. O'Keefe, "Current concepts review: the biology of the growth plate," *J. Bone Joint Surg. Ser. A* **85**(4), 715–726 (2003).
2. J. Melrose et al., "The use of Histochoice™® for histological examination of articular and growth plate cartilages, intervertebral disc and meniscus," *Biotech. Histochem.* **83**(1), 47–53 (2008).
3. B. F. Eames, L. De la Fuente, and J. A. Helms, "Molecular ontogeny of the skeleton," *Birth Defects Res. Part C* **69**(2), 93–101 (2003).

4. V. Abad et al., "The role of the resting zone in growth plate chondrogenesis," *Endocrinol.* **143**(5), 1851–1857 (2002).

5. E. Mau et al., "PTHrP regulates growth plate chondrocyte differentiation and proliferation in a Gli3 dependent manner utilizing hedgehog ligand dependent and independent mechanisms," *Dev. Biol.* **305**(1), 28–39 (2007).

6. M. Sandberg and E. Vuorio, "Localization of types I, II, and III collagen mRNAs in developing human skeletal tissues by in situ hybridization," *J. Cell Biol.* **104**(4), 1077–1084 (1987).

7. T. H. Vu et al., "MMP-9/gelatinase B is a key regulator of growth plate angiogenesis and apoptosis of hypertrophic chondrocytes," *Cell* **93**(3), 411–422 (1998).

8. F. Burdan et al., "Morphology and physiology of the epiphyseal growth plate," *Folia Histochem. Cytobiol.* **47**(1), 5–16 (2009).

9. N. B. Colthup, L. H. Daly, and S. E. Wiberly, *Introduction to Infrared and Raman Spectroscopy*, Academic Press, New York (1990).

10. P. Hendra, C. Jones, and G. Warnes, *Fourier Transform Raman Spectroscopy*, Ellis Horwood, Chichester (1991).

11. B. Schrader, *Infrared and Raman Spectroscopy: Methods and Applications*, Verlag Chemie, Weinheim (1995).

12. D. I. Ellis and R. Goodacre, "Metabolic fingerprinting in disease diagnosis: biomedical applications of infrared and Raman spectroscopy," *Analyst* **131**(8), 875–885 (2006).

13. I. Notingher et al., "In situ characterisation of living cells by Raman spectroscopy," *Spectrosc.* **16**(2), 43–51 (2002).

14. G. J. Puppels et al., "Laser irradiation and Raman spectroscopy of single living cells and chromosomes: sample degradation occurs with 514.5 nm but not with 660 nm laser light," *Exp. Cell Res.* **195**(2), 361–367 (1991).

15. G. J. Puppels et al., "Studying single living cells and chromosomes by confocal Raman microspectroscopy," *Nature* **347**(6290), 301–303 (1990).

16. H. J. Van Manen, A. Lenferink, and C. Otto, "Noninvasive imaging of protein metabolic labeling in single human cells using stable isotopes and Raman microscopy," *Anal. Chem.* **80**(24), 9576–9582 (2008).

17. V. V. Pully et al., "Hybrid Rayleigh, Raman and TPE fluorescence spectral confocal microscopy of living cells," *J. Raman Spectrosc.* **41**(6), 599–608 (2010).

18. A. Kunstar et al., "Raman microspectroscopy: a non-invasive anlysis tool for monitoring of collagen-containing extracellular matrix formation in a medium-throughput culture system," *Tissue Eng.* **17**(7), 737–744 (2011).

19. N. Uzunbajakava et al., "Nonresonant confocal Raman imaging of DNA and protein distribution in apoptotic cells," *Biophys. J.* **84**(6), 3968–3981 (2003).

20. H. J. Van Manen et al., "Intracellular chemical imaging of heme-containing enzymes involved in innate immunity using resonance Raman microscopy," *J. Phys. Chem. B* **108**(48), 18762–18771 (2004).

21. L. Hartsuiker, "Microspectroscopic characterisation of gold nanorods for cancer cell detection," PhD thesis (University of Twente: Enschede, The Netherlands, 2011).

22. N. Uzunbajakava, J. Greve, and C. Otto, "Raman microscopy of cells: chemical imaging of apoptosis," *Proc. SPIE* **4963**, 223–230 (2003).

23. C. Hervada-Sala and E. Jarauta-Bragulat, "A program to perform Ward's clustering method on several regionalized variables," *Comput. Geosci.* **30**(8), 881–886 (2004).

24. V. V. Pully, "From cells to bone: Raman microspectroscopy of the mineralization of stromal cells," PhD thesis (University of Twente: Enschede, The Netherlands, 2010).

25. I. Notingher et al., "In situ spectral monitoring of mRNA translation in embryonic stem cells during differentiation in vitro," *Anal. Chem.* **76**(11), 3185–3193 (2004).

26. S. Wold, K. Esbensen, and P. Geladi, "Principal component analysis," *Chemom. Intell. Lab. Syst.* **2**(1–3), 37–52 (1987).

27. E. Ó. Faoláin et al., "Raman spectroscopic evaluation of efficacy of current paraffin wax section dewaxing agents," *J. Histochem. Cytochem.* **53**(1), 121–129 (2005).

28. C. Y. Wang et al., "Diagnosis of oral cancer by light-induced autofluorescence spectroscopy using double excitation wavelengths," *Oral Oncol.* **35**(2), 144–150 (1999).

29. C. Krafft et al., "Near infrared Raman spectra of human brain lipids," *Spectrochim. Acta Part A* **61**(7), 1529–1535 (2005).

30. W. D. Hergeth, "Raman scattering on polymeric dispersions," *Chem. Eng. Technol.* **21**(8), 647–651 (1998).

31. K. A. Dehring et al., "Correlating changes in collagen secondary structure with aging and defective type II collagen by Raman spectroscopy," *Appl. Spectrosc.* **60**(4), 366–72 (2006).

32. S. Koljenovic et al., "Raman microspectroscopic mapping studies of human bronchial tissue," *J. Biomed. Opt.* **9**(6), 1187–1197 (2004).

33. E. David-Vaudey et al., "Fourier transform infrared imaging of focal lesions in human osteoarthritic cartilage," *Eur. Cell Mater.* **10**, 51–60 (2005).

34. W. T. Cheng et al., "Micro-Raman spectroscopy used to identify and grade human skin pilomatrixoma," *Microsc. Res. Tech.* **68**(2), 75–79 (2005).

35. E. Ó. Faoláin et al., "A study examining the effects of tissue processing on human tissue sections using vibrational spectroscopy," *Vib. Spectrosc.* **38**(1–2), 121–127 (2005).

36. R. Ellis, E. Green, and C. P. Winlove, "Structural analysis of glycosaminoglycans and proteoglycans by means of Raman microspectrometry," *Connecti. Tissue Res.* **50**(1), 29–36 (2009).

37. A. Bonifacio et al., "Chemical imaging of articular cartilage sections with Raman mapping, employing uni- and multi-variate methods for data analysis," *Analyst* **135**(12), 3193–3204 (2010).

38. M. Pudlas et al., "Non-invasive identification of proteoglycans and chondrocyte differentiation state by Raman microspectroscopy," *J. Biophotonics* 1–8 (2012).

39. C. J. Frank, R. L. Mccreery, and D. C. B. Redd, "Raman-spectroscopy of normal and diseased human breast tissues," *Anal. Chem.* **67**(5), 777–783 (1995).

40. R. J. Lakshmi et al., "Tissue Raman spectroscopy for the study of radiation damage: brain irradiation of mice," *Radiat. Res.* **157**(2), 175–182 (2002).

41. I. Notingher et al., "Discrimination between ricin and sulphur mustard toxicity in vitro using Raman spectroscopy," *J. R. Soc., Interface* **1**(1), 79–90 (2004).

42. A. J. Ruiz-Chica et al., "Characterization by Raman spectroscopy of conformational changes on guanine-cytosine and adenine-thymine oligonucleotides induced by aminooxy analogues of spermidine," *J. Raman Spectrosc.* **35**(2), 93–100 (2004).

43. M. F. K. Fung et al., "Pressure-tuning Fourier transform infrared spectroscopic study of carcinogenesis in human endometrium," *Biospectrosc.* **2**(3), 155–165 (1996).

44. C. P. Tarnowski, M. A. Ignelzi, and M. D. Morris, "Mineralization of developing mouse calvaria as revealed by Raman microspectroscopy," *J. Bone Miner. Res.* **17**(6), 1118–1126 (2002).

45. J. W. Chan et al., "Micro-Raman spectroscopy detects individual neoplastic and normal hematopoietic cells," *Biophys. J.* **90**(2), 648–656 (2006).